Electronic structures and magnetic couplings of B-, C-, and N-doped BeO*

Pang Hua(庞 华)†, Zhang Sha(张 莎), and Li Fa-Shen(李发伸)

Key Laboratory for Magnetism and Magnetic Materials of the Ministry of Education, Lanzhou University, Lanzhou 730000, *China*

(Received 5 June 2012; revised manuscript received 7 September 2012)

The electronic structures and magnetic properties of B-, C-, and N-doped BeO supercells are investigated by means of *ab initio* calculations using density functional theory. The magnetic exchange constants of C-doped BeO at different doping levels are also calculated. A phenomenological band structure model based on p–d exchange-like p–p level repulsion between the dopants is proposed to explain the magnetic ground states in B-, C-, and N-doped BeO systems. The evolution from the antiferromagnetic phase to the ferromagnetic phase of C-doped BeO supercell with C concentration decreasing can also be well explained using this model. The findings in this study provide a simple guide for the design of band structure for a magnetic sp-electron semiconductor.

Keywords: electronic structure, magnetic coupling, first-principles

PACS: 75.30.Hx, 71.20.–b, 71.15.Mb **DOI:** 10.1088/1674-1056/22/4/047504

1. Introduction

Recently, magnetism involving only s- and p-electron elements has received much attention from both fundamental research and potential applications. The defect-induced magnetism in the carbon nano-tube has been extensively studied.[1,2] The magnetic order in a three-dimensional graphitic network with single atom vacancies can be attributed to the polarization of C p states.[3] The magnetism in BN sheet due to nonmagnetic impurities proves the possibility of magnetism in pure sp-electron alloys with reduced dimensions.[4,5] The dilute magnetic semiconductors (DMSs) with nonmagnetic dopants, such as Cu-doped ZnO,[6] C-doped ZnO,[7] Cu-doped GaN,[8] Cu-doped TiO,[9] B-doped ZnO,[10] N-doped ZnO,[11] etc., are proved to be room-temperature DMSs experimentally, where the p–d exchange-like p–p coupling interaction and the hole-mediated double exchange mechanism are suggested to be responsible for the ferromagnetism.[12–15] However, to our knowledge, the physical mechanism of the emergence of magnetism in these materials is not well understood, partly due to the conflicting experimental reports.[16–19]

In this paper we aim to explore the possible mechanism of magnetic couplings in sp-electron semiconductors using a simple band structure model. We show through first principles calculations that this model can successfully explain the magnetic ground states of B-, C-, and N-doped BeO systems.

2. Calculation methods

The first-principles calculations are performed using the full-potential linearized augmented plane-wave (FLAPW) method based on density functional theory. All calculations are carried out using the Wien2k package.[20] The values of muffin-tin radius ($R_{\rm mt}$) of Be and O are chosen to be 1.60 a.u. and 1.50 a.u. (The abbreviation a.u. is short for atomic unit), respectively. For B, C, and N, the values of $R_{\rm mt}$ are chosen to be 1.70, 1.65, and 1.60 a.u., respectively. The value of the cutoff of wave function ($K_{\rm max}$) multiplied by the radius of atom ($R_{\rm mt}$), i.e., ($R_{\rm mt} \times K_{\rm max}$), is set to be 7.0 and the magnitude of the largest vector $G_{\rm max}$ to be 14.0. For the exchange–correlation functional, we employ the generalized gradient approximation (GGA) (Perdew–Burke–Wang form) in all calculations. Due to the intrinsic limitation, the GGA band gap energy of bulk BeO is 7.4 eV, strongly underestimating the measured gap of 10.6 eV.[21,22] Nevertheless, the electronic structures near and below the Fermi surface are accurate using the GGA method.

Pure BeO has a wurzite structure. The optimized lattice constants, a and c, of the BeO unit cell are 2.705 Å (1 Å = 0.1 nm) and 4.384 Å, respectively. Both are slightly larger than the experimental values.[23] Based on this unit cell, a 2×2×2 supercell containing 32 atoms is constructed and a defect is introduced by substituting a dopant atom D (D = B, C, and N) for an O atom, corresponding to a doping level of 6.25%. To investigate the evolution of magnetic ordering of the C-doped BeO system with the doping level, four supercells, i.e. 2×2×1, 2×2×2, 3×3×1, and 3×3×2, are constructed and a defect is introduced into each supercell by substituting a C atom for an O atom, corresponding to the doping levels of 12.50%, 6.25%, 5.56%, and 2.27%, respectively. To study the magnetic exchange interactions in the C-doped BeO system, four magnetic ordered configurations are set up based on the supercells mentioned above. Figure 1 displays the mag-

*Project supported by the National Natural Science Foundation of China (Grant No. 10975066).

†Corresponding author. E-mail: hpang@lzu.edu.cn

© 2013 Chinese Physical Society and IOP Publishing Ltd

netic configurations of BeO supercells with 6.25% C doping, where the small white balls represent Be atoms and the other small balls refer to O atoms. The C atoms are denoted by big balls and those with the same color couple ferromagnetically. For simplicity, the four configurations are called AFMx, AFMxz, AFMz, and FM states respectively. The corresponding unit-cell of each magnetic configuration is also shown in the inset of Fig. 1.

The doped structures are optimized with respect to both the lattice constants and the atomic positions. Atomic coordinates are fully relaxed using the conjugate-gradient algorithm until the maximum force on a single atom is less than 1 mRy/Å (1 Ry = 13.605 eV). The $\boldsymbol{k}$ mesh convergence tests are also performed for each system. For example, a gamma-centered 6×6×3 $\boldsymbol{k}$ mesh is used to sample the irreducible Brillouin zone in the defect calculation for the 2×2×2 supercell. Convergence tests are performed by 5×5×3 $\boldsymbol{k}$ mesh and 7×7×5 $\boldsymbol{k}$ mesh, by which the obtained total energies differ by less than 1 meV.

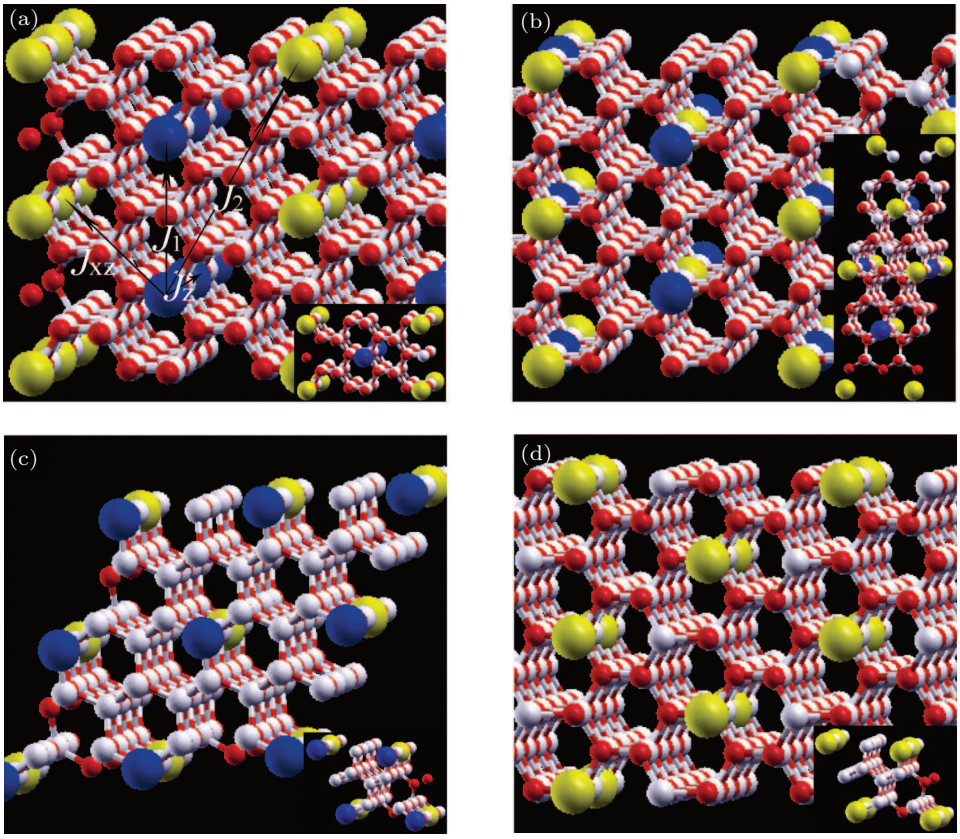


Fig. 1. (color online) Magnetic configurations and the proposed magnetic couplings (see text) of 6.25% C-doped BeO supercells. (a) AFMx, (b) AFMxz, (c) AFMz, (d) FM. The inset shows its corresponding unit-cell of each magnetic configuration.

3. Results and discussion

In doped BeO, the dopant atom D is in a non-regular tetrahedral cage of four Be atoms. Three first nearest neighbors of D (named Be_1 hereafter) construct the basal plane of the tetrahedron and the second nearest neighbor (named Be_2) is located at the top of the tetrahedron. Considering that the radii of atoms B, C, and N are close to the radius of O when they are in tetrahedral covalent bonds, one would not expect strong structural relaxation through substituting. This is indeed the case. For example, lattice constant a reduces about 0.4% and c increases about 1.0% for 6.25% C-doped BeO supercell after full relaxation. In the following, as an example the systems with a dopant concentration of 6.25% are discussed unless otherwise specified.

3.1. Electronic structures and magnetic moments

For doped BeO systems, total energy calculations are performed on magnetic and non-magnetic (NM) phases. It is found that magnetization will always reduce the energy of the doped system. The spin-resolved densities of states (DOSs) of BeO supercells with different doping elements are shown in Fig. 2, as well as the DOS of the bulk BeO for reference. The NM phase is stable for bulk BeO. As shown in Fig. 2(a), the valence band is comprised of mainly oxygen p orbitals and is full, while the conduction band is composed of mainly Be s orbitals and is empty. When a substitution atom is intro-

duced, the DOS is significantly modified around the Fermi energy as shown in Figs. 2(b)–2(d). There are at least three features about the total DOS of doped BeO systems: (i) the Fermi energy level lies in the impurity band for each system and the exchange splitting of the impurity band is obvious; (ii) the electronic structures of C-doped BeO and N-doped BeO show half-metallic characteristics: the majority spin components are semiconducting while the minority spin components are metallic; (iii) the impurity band tends to connect with the main body of the host band structures with the increase of impurity p electrons, indicating stronger interaction of the doping atoms with the matrix. Our results match well with those in Refs. [24] and [25].

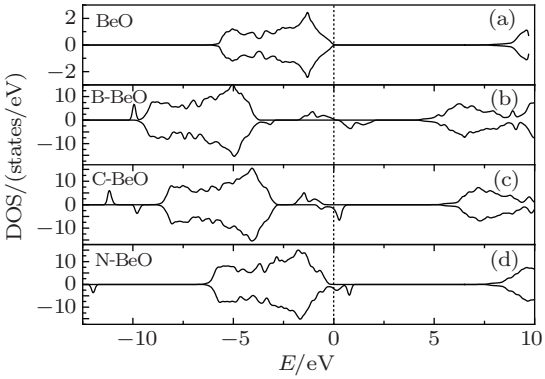


Fig. 2. Spin-resolved DOSs of bulk BeO (a) and doped supercells, each with a doping level of 6.25% ((b) to (d)).

We have investigated the distributions of magnetic moments in doped BeO supercells. With the p valence electrons of the impurity increasing from B to N, the total magnetic moment of the supercell reduces from 3.00 μ_B to 1.00 μ_B. At the same time, the magnetic moment within the muffin-tin of the impurity decreases from 0.99 μ_B for B, to 0.81 μ_B for C, and to 0.53 μ_B for N. These observations match with those of defected BeO nano-tubes reported in Refs. [25]– [27] and further suggest the conditions to realize local magnetization in doped sp-electron materials. Such as in B-, C-, and N-doped BeO supercells, the dopant atoms form covalent bonds with Be_1 and Be_2 atoms, which helps the *D*–Be tetrahedron to bind the holes introduced by B, C, and N doping, hence resulting in high spin ground state for the degenerate impurity p bands.[7] When the number of holes increases, the magnetic moment of the doping atom increases consequently.

It is found that the magnetic moments of C atom are 0.80 μ_B/atom, 0.81 μ_B/atom, 0.79 μ_B/atom, and 0.79 μ_B/atom for systems with doping level of 12.50%, 6.25%, 5.56%, and 2.27%, respectively, which are in accordance with those reported in the papers by Shein *et al*.[27,28] It seems that the influence of spin polarization of the impurity band spreads to its fifth nearest neighbor. Take the 5.56% C-doped BeO for example, the magnetic moments are 0.04 μ_B/atom, 0.08 μ_B/atom, 0.07 μ_B/atom, 0.07 μ_B/atom, and 0.02 μ_B/atom from the first nearest neighbor to the fifth nearest neighbor of C in turn. No noticeable magnetic moments are found from other atoms.

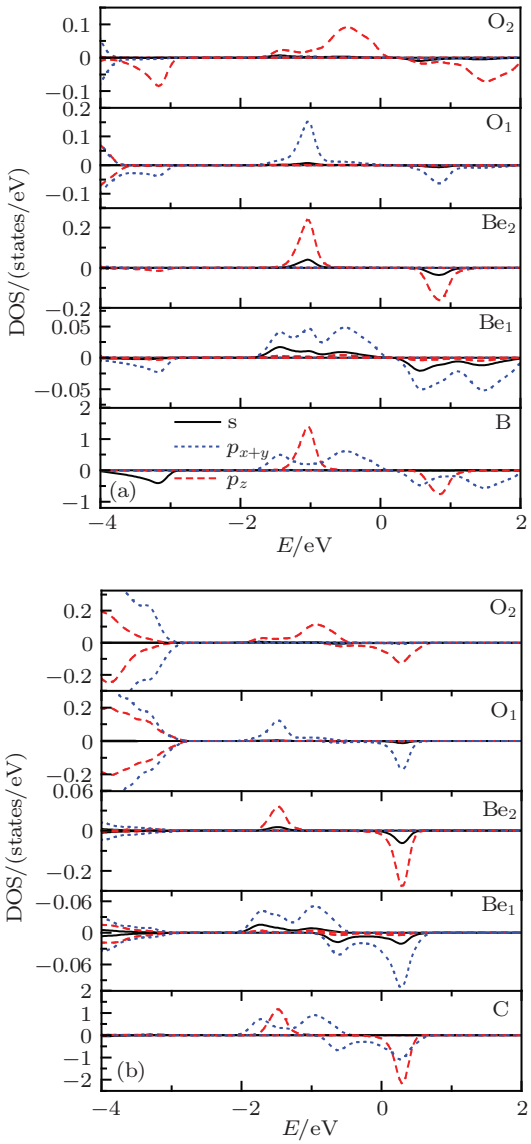


Fig. 3. (color online) Partial DOSs of the dopant and its neighbor sites in B-doped (a) and C-doped (b) supercells.

The partial DOSs of the dopants and their neighbors make it clear that for B-, C-, and N-doped BeO, the local moment of impurity originates from the high spin ground state of the impurity p bands. Figures 3(a) and 3(b) show the partial DOS of B-doped BeO and that of C-doped BeO, respectively. The situation for N-doped BeO is similar to that of C-doped BeO near the Fermi level, hence it is not shown. We see that for both cases the states near the Fermi level are composed of impurity p bands and the valence bands (comprised mainly of Be p and O p bands) of its neighbors. Obviously, the spin polarization of the impurity p state results in the magnetic moment of the dopant. As to Be_1 and Be_2 sites, polarized Be s and Be p states contribute most to the magnetic moment, and the polarized O p states near the Fermi level account for the moments of the O neighbors.

3.2. Magnetic ground state and the model of magnetic coupling

We then come to the magnetic ground states of the doped BeO systems. Total energy calculations are performed with two impurity atoms in ferromagnetic (FM) and antiferromagnetic (AFM) states for each doped supercell. The values of energy difference ΔE ($\Delta E = E^{\mathrm{AFM}} - E^{\mathrm{FM}}$) are listed in Table 1. We see that the magnetic ground state of the supercell is sensitive to the doping element and the doping level. At 6.25% doping level, only N-doped BeO has FM ground state. While for C-doped BeO systems, with C content decreasing, the magnetic ground state is converted from AFM state into FM state.

Table 1. Values of total energy difference $\Delta E_i = E^i - E^{\mathrm{FM}i}$ (meV/f.u.) between two magnetic coupling states and the magnetic ground states for the doped BeO supercells.

Dopant	%	$\Delta E_{\mathrm{AFM}x}$	$\Delta E_{\mathrm{AFM}z}$	$\Delta E_{\mathrm{AFM}xz}$	Ground state
B	6.25	–140.0	–0.5	–247.0	AFM
C	12.5	1386.9	–3.4	208.3	AFM
	6.25	195.8	–0.8	222.6	AFM
	5.56	3.9	3.9	21.2	FM
	2.27	–	50.3	–	FM
N	6.25	18.7	2.0	93.8	FM

Transition metal (TM) doped diluted magnetic semiconductors have been extensively studied. A unified band coupling model based on the p–d and d–d level repulsions between the TM and host elements is proved to be successful in explaining the charge-induced ferromagnetism,[29,30] while in sp-electron alloys, it has been proposed that the long-range magnetic coupling results from the p–p interaction and that the competition between double exchange and super-exchange interactions is widely used when discussing the magnetic ground states.[7] But in view of band structure, the discussion is ambiguous and lacking in universality. Here we suggest a phenomenological band structure model based on p–d exchange-like p–p level repulsion between the sp-electron dopants. This model can successfully explain the magnetic ordering in doped BeO systems.

For B-, C-, and N-doped BeO systems as shown in Fig. 2, the Fermi levels are within the impurity p bands which are above the valence band maximum of the host p states. As is well known, the states with the same symmetry can couple strongly with each other and without spin–orbit coupling, only the states with the same spin configuration can couple with each other.[29] Thus the host p band and the impurity p band can form symmetry-allowed p–p coupling, and the coupling leads to a level repulsion that pushes up the impurity p band by $\Delta^{\alpha}_{\mathrm{pp}}$ and pushes down the host p state by the same amount, which is shown schematically in Fig. 4(a). Coupling also happens between the impurity p states. For neighboring dopant atoms, the p–p coupling between the same spin states leads to splittings $2\Delta^{1}_{\mathrm{pp}}$ and $2\Delta^{2}_{\mathrm{pp}}$ as shown in Figs. 4(b) and 4(c). However, the coupling between the majority p state and the minority p state pushes up the minority state by $\Delta^{12}_{\mathrm{pp}}$ and pushes down the majority state by the same amount as shown in Fig. 4(d).

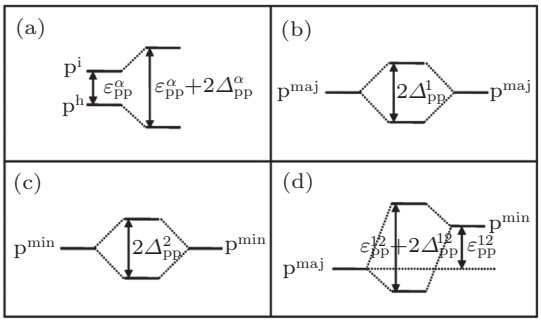


Fig. 4. (color online) Schematic diagrams of model for p–p couplings. (a) p–p coupling between host p band and the impurity p band. (b) p–p coupling between impurity p majority states. (c) p–p coupling between impurity p state and minority state. (d) p–p coupling between majority p state and minority p state.

According to Fig. 4, there will be no energy gain if the two coupled states are both fully occupied or both fully empty, and the p–p coupling between host p band and impurity p band results in the same energy gain separately in FM configuration and in AFM configuration, therefore it is ineffective in determining the magnetic ground state. Hence only p–p coupling between the dopant p states is considered in the following discussion.

For details, we start from the situation that the majority states of the impurity band are full and the minority states are empty. B-doped BeO system belongs to this case. Figure 5(a) shows the p–p level repulsions for the AFM and FM configurations of B-doped BeO system. In this case, the energy gain for the AFM configuration is $-2n_1\Delta^{12}_{\mathrm{pp}}$, where n_1 is the number of electrons of the majority states. While for the FM configuration, no energy gain is obtained since the majority states are fully occupied. Hence the energy difference between the FM and AFM configurations is $\Delta E_{\mathrm{FM-AFM}} = 2n_1\Delta^{12}_{\mathrm{pp}}$. Obviously, the AFM state is stabilized.

If the majority states are full and the minority states are partially filled as shown in Fig. 5(b), the energy gain is $-2n_{\mathrm{e}}\Delta^{2}_{\mathrm{pp}}$ for the FM configuration, where n_{e} is the number of electrons of the minority states. For the AFM phase, the energy gain is $-2[(n_1 - n_{\mathrm{e}})\Delta^{12}_{\mathrm{pp}}]$. Thus the energy difference between the two configurations is

$$\Delta E_{\mathrm{FM-AFM}} = -2n_{\mathrm{e}}\Delta^{2}_{\mathrm{pp}} + 2[(n_1 - n_{\mathrm{e}})\Delta^{12}_{\mathrm{pp}}] \qquad (1)$$

or

$$\Delta E_{\mathrm{FM-AFM}} = -2(n_2 - n_{\mathrm{e}})\Delta^{2}_{\mathrm{pp}} + 2[(n_1 - n_{\mathrm{e}})\Delta^{12}_{\mathrm{pp}}] \cdots (n_{\mathrm{e}} \geq n_2/2)\,, \qquad (2)$$

where n_2 is the total number of electrons in the minority states. Then it is possible that the FM configuration is stabilized by

a suitable value of n_e. The C- and N-doped BeO systems are good examples as shown in Fig. 2. The electrons are introduced into the impurity minority bands and N-doped BeO reaches FM ordering.

Actually, figure 5(a) is the case for super-exchange dominated coupling, which usually results in AFM coupling. Figure 5(b) depicts the situation where the double exchange mechanism works. Hence it is reasonable to assume that the first term in Eq. (1) represents the double exchange term, and the second is the super-exchange term. Our model makes it clear that the magnetic ground state is highly sensitive to the property and the number of charge carriers in sp-electron semiconductors, and that an FM state can be stabilized only if there are both holes and electrons in the coupled states. For example, the B-doped BeO system has an AFM ground state according to DFT calculations. If there are enough additional electrons for each B atom that the impurity minority states are partially occupied, then according to Eq. (1), FM phase is possible. There is also the chance that holes are introduced into the impurity majority bands and the minority states are empty as shown in Fig. 5(c). Then the energy difference between the FM and AFM phases can be written as $\Delta E_{\mathrm{FM-AFM}} = -2n_{\mathrm{h}}\Delta^{1}_{\mathrm{pp}} + 2[(n_1 - n_{\mathrm{h}})\Delta^{12}_{\mathrm{pp}}]$, where n_{h} is the number of holes. Accordingly, the increasing of n_{h} is in favor of FM coupling.

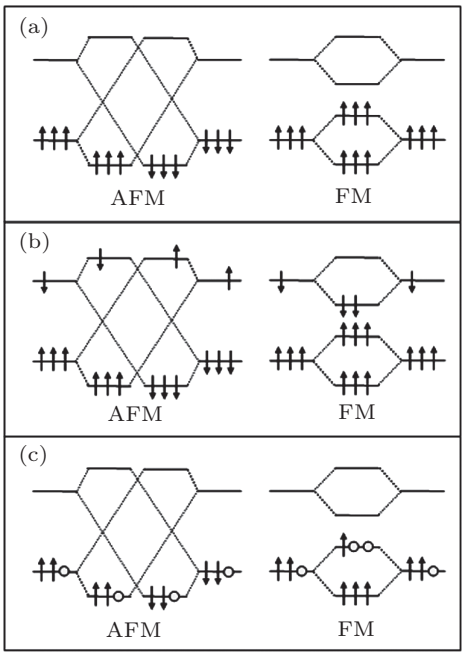


Fig. 5. Couplings in AFM and FM configurations of impurity doped BeO system for the cases: (a) the impurity majority states are full and the minority states are empty; (b) the impurity majority states are full and the minority states are partially filled; (c) the holes are introduced into the impurity majority bands and the minority states are empty.

The evolution of the magnetic ground state with the decrease of C content for C-doped BeO system can also be well explained according to Eq. (1). The first term in Eq. (1) stabilizes the FM phase while the second term stabilizes the AFM phase. Figure 6 gives the total DOSs of C-doped BeO systems with different values of C content. We see that the band width of each C p orbital becomes narrower with the reduction of C content due to the decreasing of crystal field splitting, which reduces Δ^{2}_{pp}. At the same time, the exchange splitting of C p orbital increases, which reduces $\Delta^{12}_{\mathrm{pp}}$. However, at low C concentration, the exchange splitting is larger than the crystal field splitting for C p state, hence the FM interaction Δ^{2}_{pp} is larger than the AFM interaction $\Delta^{12}_{\mathrm{pp}}$.[29] When the doping level is less than 6.25%, the C p state is completely spin polarized, which dramatically lowers $\Delta^{12}_{\mathrm{pp}}$ and the FM phase is reached. Our observations suggest that the magnetic ground state is also sensitive to the exchange splitting and the crystal field splitting of the impurity band for the sp-material.

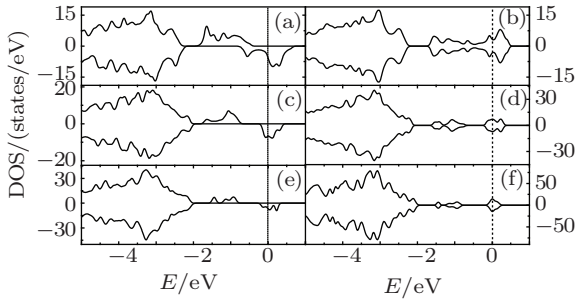


Fig. 6. DOS comparison between antiferromagnetic states (left column) and ferromagnetic states (right column) of C-doped BeO supercells with different C concentration: 12.5% ((a) and (b)), 5.56% ((c) and (d)), and 2.27% ((e) and (f)).

3.3. Magnetic exchange constant

To explore the magnetic exchange constant, the computations of total energies for supercells characterized by different collinear spin arrangements of the C moments are performed, and an Ising-like Hamiltonian is used to describe the magnetic excitation in C-doped BeO supercell, as $\hat{H} = \hat{H}_0 + \sum_{i>j} J_{ij}\hat{S}_i\hat{S}_j$, where $\hat{H}_0$ represents the spin-independent part of the Hamiltonian, $\hat{S}_i$ and $\hat{S}_j$ stem from the spin-1/2 operators localized on C sites i and j, respectively, and J_{ij} is the magnetic coupling between these moments.[31] Here the summation over i and j extends over the sites in the C sublattice, and the magnetic moment of each site is set to be the same for convenience.

As shown in Fig. 1, magnetic coupling up to the second-nearest neighbor within the xy-plane of the system, denoted as J_1 and J_2, and the interlayer interactions up to the second-nearest neighbor, represented by J_z and J_{xz}, are evaluated. In the following, the intra-layer interaction is simplified as $J_{xy} = (J_1 + J_2)$, which is justified by the similarities in the double exchange pathways associated with J_1 and J_2. To calculate three kinds of magnetic couplings, $2^3 = 8$ possible configurations are needed since there are two C atoms in each AFM unit-cell. Spin reversal and crystalline symmetry reduce

this number to 4. Three kinds of antiferromagnetic configurations, named AFMx, AFMxz, AFMz, are constructed as shown in Fig. 1. Due to the different magnetic structures, the three AFM configurations have different crystal symmetries and unit-cells. Hence for each AFM configuration, an FM configuration is constructed using the same unit-cell. An example is given in Fig. 1(d), which shows the FM state of AFMx configuration. In this way, the total energy difference between the FM state and the AFM state with the same unit-cell ($\Delta E = E - E^{\mathrm{FM}}$) can be ascribed to the different magnetic coupling between local moments of the two states. In terms of exchange constants, ΔE for the three antiferromagnetic configurations, AFMx, AFMxz, AFMz, can be described as $4J_{xy} + 8J_{xz}$, $4J_{xy} + 2J_z + 4J_{xz}$, and $2J_z + 12J_{xz}$, respectively.

Magnetic couplings for C-doped BeO supercells at different doping levels finally obtained based on the magnetic configurations shown in Fig. 1 are listed in Table 2. Obviously, for each doping level, the exchange coupling is anisotropy in nature. We see for all doping systems, J_{xy} and J_z are negative, indicating FM coupling for C atoms in the same xy-plane and along the c axis. While the cross interlayer exchange coupling J_{xz} is positive, indicating AFM ordering. It is found that all couplings have short range characteristics. For example, when d_z and d_{xy} increase in 5.56% C-doped system compared with that in 12.5% C-doped system as shown in Table 2, the three couplings decrease in values distinctly and the decreasing in J_{xy} is most pronounced. Actually, it seems that all couplings are more sensitive to the intra-layer distance between the impurities than the interlayer distance. The anisotropy and short-range nature of the exchange coupling suggest that the distribution of the impurity is another key factor influencing the magnetic ground state of the system.

Table 2. Magnetic couplings in C-doped BeO system. (d_z is the distance between two nearest C atoms along the c axis; and d_{xy} is the distance between the two nearest C atoms in the in-plane; a and c are lattice constants).

Doping level/%	d_{xy}	d_z	J_{xy}/meV	J_z/meV	J_{xz}/meV
12.5	$2a$	c	–22.10	–12.98	2.31
6.25	$2a$	$2c$	–26.20	–4.97	0.86
5.56	$3a$	$2c$	–1.32	–3.50	0.42

4. Conclusion

In this paper, the magnetic properties of B-, C-, and N-doped BeO supercells are studied from first principles using an FPLAPW and GGA method. Based on p–p coupling and level repulsion between the dopant p states, a model is proposed to explain the magnetic ordering of sp-electron semiconductor. The model can be easily related to the competition between double exchange and super-exchange interactions, hence the band structure of the material. It is found that the magnetic state of sp-material is sensitive to the properties and quantity of the charges as well as the distribution of the defects. Our results will be helpful for understanding the different experimental reports about the magnetic ground state of even the same material, since the details of the synthesis process will strongly influence the spatial homogeneity of the impurities and the properties of the charge carriers.

References

[1] Li F, Zhu Z H, Yao X D, Lu G Q, Zhao M W, Xia Y Y and Chen Y 2008 *Appl. Phys. Lett.* **92** 102515
[2] Ma Y, Foster A S, Krasheninnikov A V and Nieminen R M 2005 *Phys. Rev. B* **72** 205416
[3] Faccio R, Pardo H, Denis P A, Yoshikawa Oeiras R, Araújo-Moreira F M, Veríssimo-Alves M and Mombrú A W 2008 *Phys. Rev. B* **77** 035416
[4] Si M S and Xue D S 2007 *Phys. Rev. B* **75** 193409
[5] Singh R and Kroll P 2009 *J. Phys.: Condens. Matter* **21** 196002
[6] Hou D L, Ye X J, Meng H J, Zhou H J, Li X L, Zhen C M and Tang G D 2007 *Appl. Phys. Lett.* **90** 142502
[7] Pan H, Yi J B, Shen L, Wu R Q, Yang J H, Lin J Y, Feng Y P, Ding J, Van L H and Yin J H 2007 *Phys. Rev. Lett.* **99** 127201
[8] Lee J H, Choi I H, Shin S, Lee S, Lee J, Whang C, Lee S C, Lee K R, Baek J H, Chae K H and Song J H 2007 *Appl. Phys. Lett.* **90** 032504
[9] Duhalde S, Vignolo M F, Chiliotte C, Rodríguez Torres C E, Errico L A, Cabrera A F, Rentería M, Sánchez F H and Weissmann M 2005 *Phys. Rev. B* **72** 161313
[10] Xu X G, Yang H L, Wu Y, Zhang D L and Jiang Y 2012 *Chin. Phys. B* **21** 047504
[11] Wen Z, Wu D, Gao J L, Tang S L, Xu Q Y, Qiu T and Xu M X 2011 *Chin. Phys. B* **20** 087505
[12] Ma Y D, Dai Y and Huang B B 2011 *Comput. Mater. Sci.* **50** 1661
[13] Zhang C W, Wang P J and Li P 2011 *Solid State Sci.* **13** 480
[14] Pan H, Feng Y P, Wu Q Y, Huang Z G and Lin J Y 2008 *Phys. Rev. B* **77** 125211
[15] Yang K S, Wu R Q, Shen L, Feng Y P, Dai Y and Huang B B 2010 *Phys. Rev. B* **81** 125211
[16] Sudakar C, Thakur J S, Lawes G, Naik R and Naik V M 2007 *Phys. Rev. B* **75** 054423
[17] Tiwari A, Snure M, Kumar D and Abiade J T 2008 *Appl. Phys. Lett.* **92** 062509
[18] Herng T S, Lau S P, Yu S F, Yang H Y, Ji X H, Chen J S, Yasui N and Inaba H 2006 *J. Appl. Phys.* **99** 086101
[19] Nguyen H H, Virginie B and Joe S 2005 *Appl. Phys. Lett.* **86** 082505
[20] Blaha P, Schwarz K, Sorantin P and Trickey S B 1990 *Comput. Phys. Commun.* **59** 399
[21] Roessler D M, Walker W C and Loh E 1969 *J. Phys. Chem. Solids* **30** 157
[22] Griindler R, Breuer K and Tews W 1978 *Phys. Status Solidi B* **86** 329
[23] Hazen R M and Finger L W 1986 *J. Appl. Phys.* **59** 3728
[24] Baumeier B, Krüger P and Pollmann J 2007 *Phys. Rev. B* **75** 045323
[25] Shein I R, Ryzhkov M V, Gorbunova M A, Makurin Y N and Ivanovskii A L 2007 *JETP Lett.* **85** 246
[26] Gorbunova M A, Shein I R, Makurin Y N, Ivanovskaya V V, Kijko V S and Ivanovskii A L 2008 *Physica E* **41** 164
[27] Shein I R, Gorbunova M A, Kiiko V S and Ivanovskii A L 2010 *Rev. Adv. Mater. Sci.* **26** 48
[28] Shein I R, Gorbuniva M A, Makurin Y N, Kiiko V S and Ivanovskii A L 2008 *Int. J. Mod. Phys. B* **22** 4987
[29] Dalpian G M, Wei S H, Gong X G, Antonio J R, da Silva and Fazzio A 2006 *Solid State Commun.* **138** 353
[30] Walsh A, Juarez L F, da Silva and Wei S H 2008 *Phys. Rev. Lett.* **100** 256401
[31] Saúl A and Radtke G 2011 *Phys. Rev. Lett.* **106** 177203